Supplementary Information for

Divalent Organic Cations as the Novel Protective Layer for Perovskite Materials

Yan Chen,[ab] Xun-Lei Ding,[*abcd] Han-Bin He,[a] Ya-Ya Wang,[ab] Shao-Peng Xu,[ab] Meng-Meng Wang,[ab] and Wei Li[acd]

[a]   School of Mathematics and Physics, North China Electric Power University, Beinong Road 2, Changping, Beijing 102206, P. R. China.

[b]   School of New Energy, North China Electric Power University, Beinong Road 2, Changping, Beijing 102206, P. R. China.

[c]   Institute of Clusters and Low Dimensional Nanomaterials, North China Electric Power University, Beinong Road 2, Changping, Beijing 102206, P. R. China.

[d]   Hebei Key Laboratory of Physics and Energy Technology, North China Electric Power University, Baoding, 071000, China

* Author to whom correspondence should be addressed.
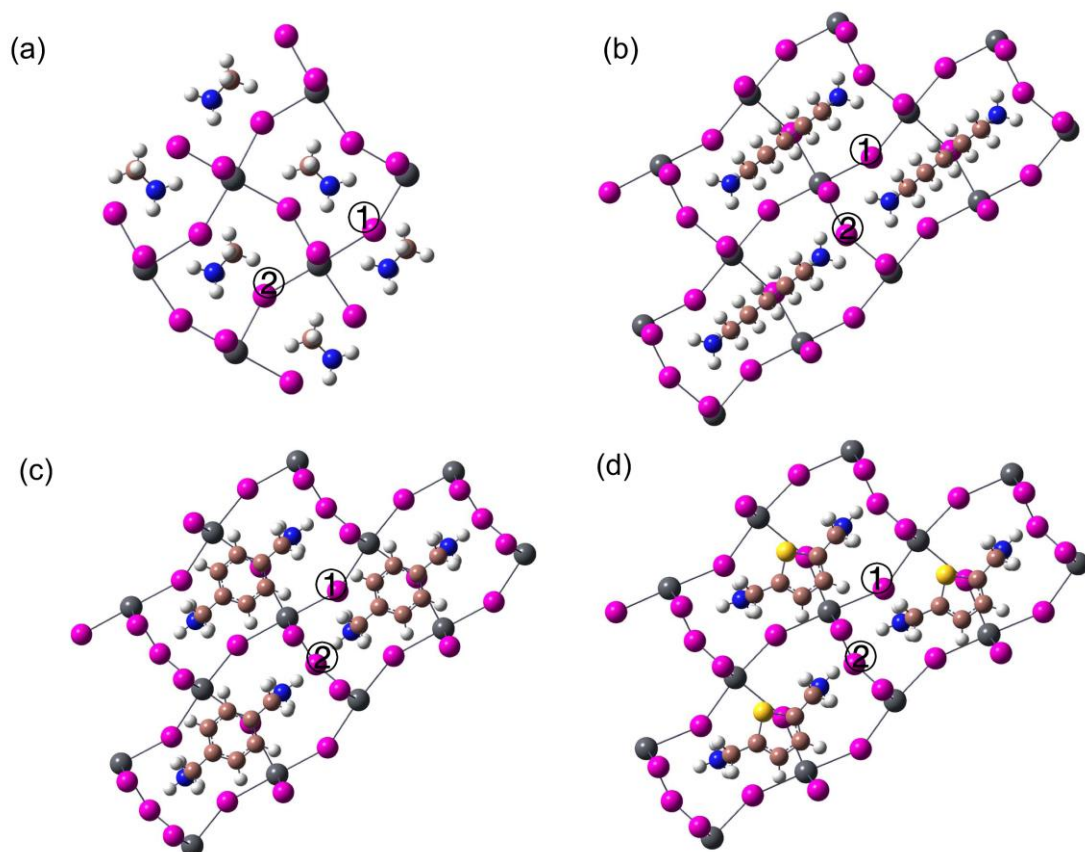   Email: dingxl@ncepu.edu.cn

Figure S1. The cluster models used for the calculations of wave functions for (a) $(MA)_2$-PS, (b) ProDMA-PS, (c) PhDMA-PS, and (d) ThDMA-PS. Labels 1 and 2 indicate two possible positions for H_2O adsorption. The cluster models consist of atoms of the first layer, including the cations and water molecules in focus, as well as the atoms around them. The number of ions in the cluster model is adjusted slightly to obtain an electrically neutral system. Density functional theory (DFT) calculations of the cluster models are performed using Gaussian 16 program suite [1] with B3LYP functional [2-4] and LANL2DZ basis set.[5] Dispersion correction [6] is involved in all calculations in order to describe the weak interaction more accurately.
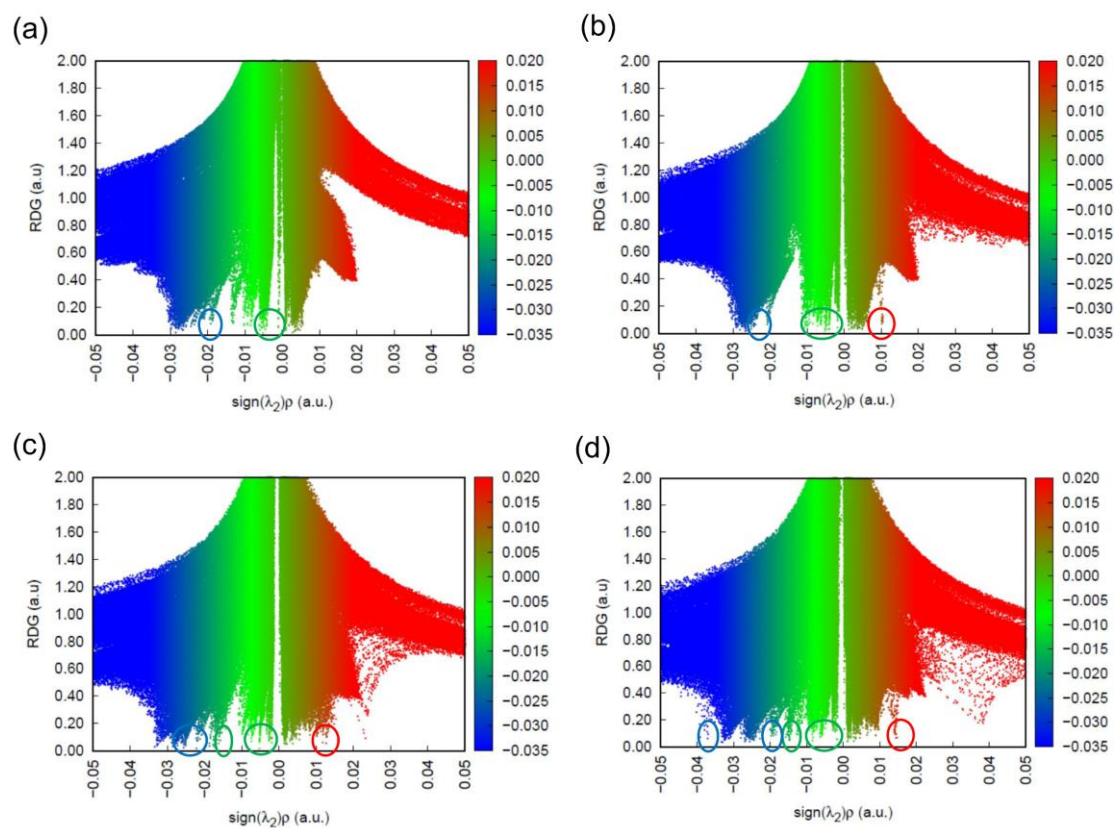
Figure S2. The color-filled sign(λ_2)ρ vs. RDG scatter map for (a) (MA)$_2$-PS, (b) ProDMA-PS, (c) PhDMA-PS, and (d) ThDMA-PS calculated by cluser models. The circles in blue, green, and red indicate the spikes for the NH···I and CH···I interactions, and repulsive interactions, respectively.
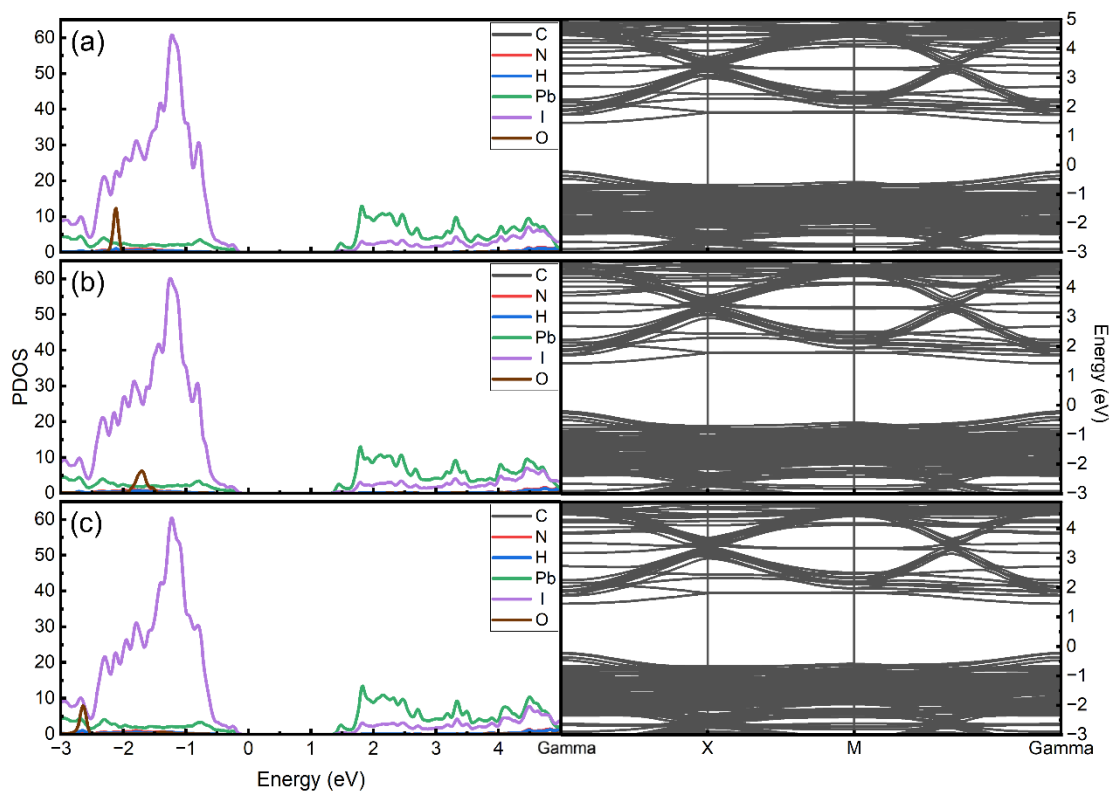
Figure S3. The partial density of states (PDOS) and band structure of ProDMA-PS with a H_2O in O-zone from (a) Site 1 and (b) Site 2, and (c) F-zone from Site 1.
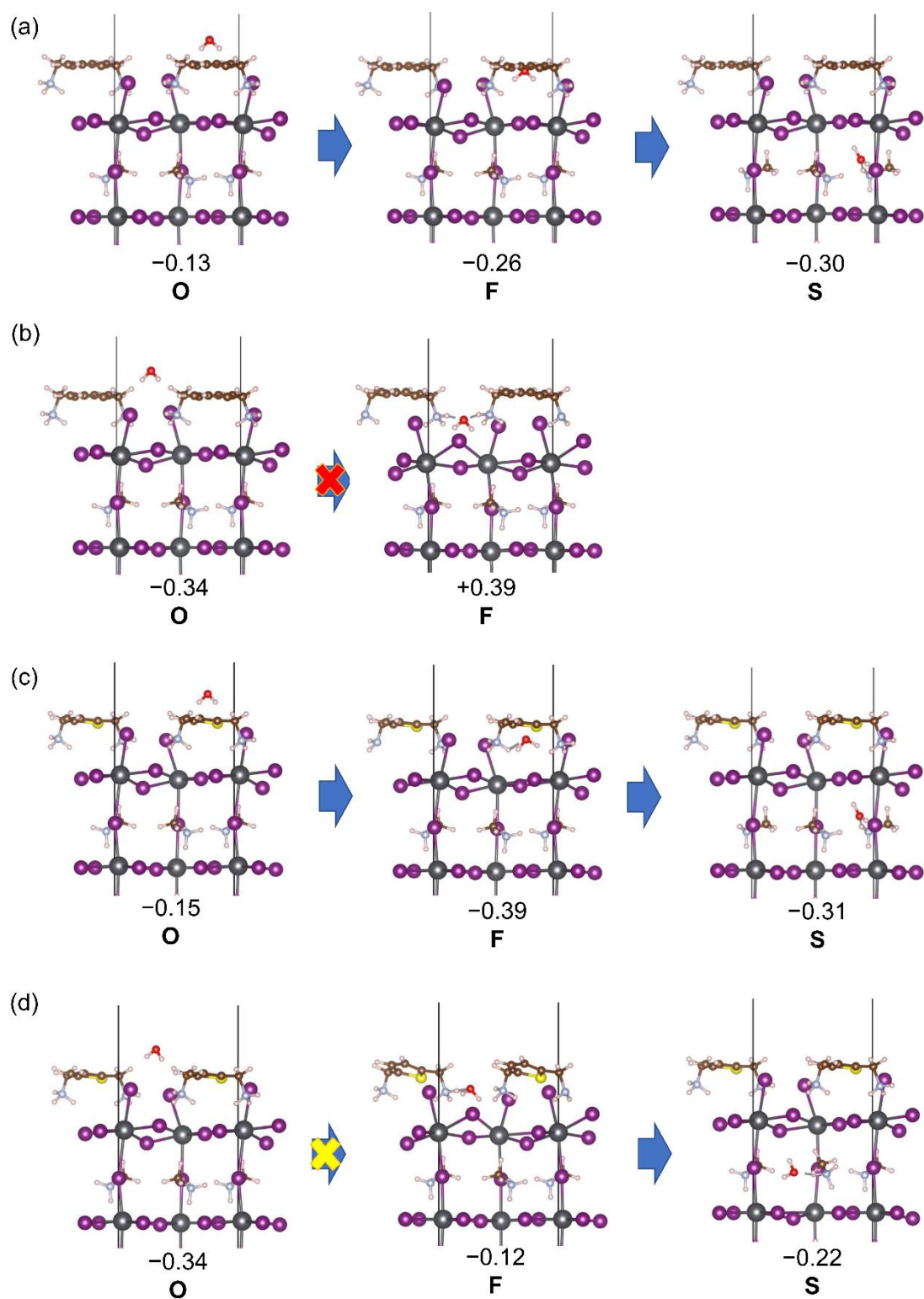
Figure S4. The invasion process of a H$_2$O on PhDMA-PS from (a) Site 1 and (b) Site 2, and on ThDMA-PS from (c) Site 1 and (d) Site 2, with the relative energy ($E_{r\text{-H2O}}$) in eV.

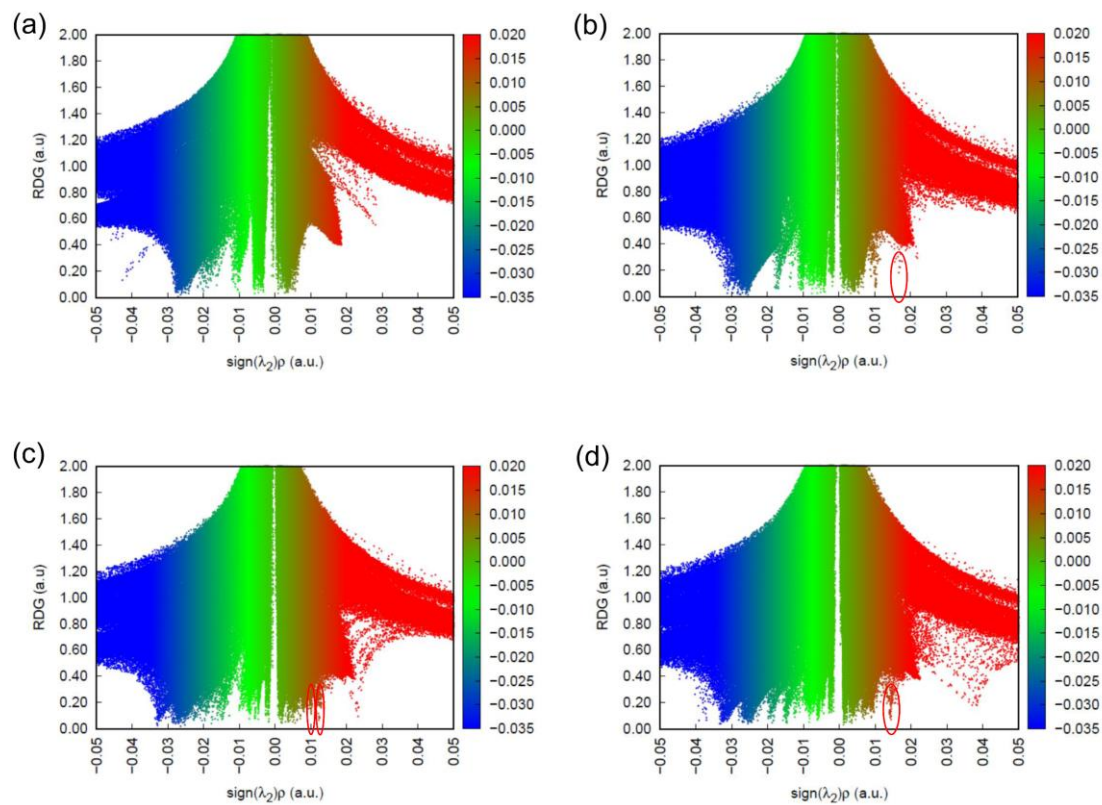Figure S5. The color-filled sign(λ_2)ρ vs. RDG scatter maps of the H$_2$O adsorbed in F-zone from Site 1 for (a) (MA)$_2$-PS, (b) ProDMA-PS, (c) PhDMA-PS, and (d) ThDMA-PS. The circles in red indicate the spikes for repulsive interactions.

Simulation of Power conversion efficiency (PCE)

The simulation of PCE for the $(MA)_2$-PS and ProDMA-PS takes the configuration of FTO/TiO$_2$/PS/MAPbI$_3$/PS/Spiro-OMeTAD/Au, where PS is either the original perovskite, $(MA)_2$-PS, or the modified one, ProDMA-PS (Figure S6). The parameters of materials TiO$_2$, MAPbI$_3$, Spiro-OMeTAD, and interface defect layers (TiO$_2$/light-harvester and light-harvester/Spiro-OMeTAD) are obtained from the research of Raoui *et al.*[7] The parameters of materials $(MA)_2$-PS and ProDMA-PS are calculated by the following definitions. The parameters are summarized in Tables S1 and S2. The structure is illuminated from the top at normal incidence using the standard AM 1.5G spectrum (1 kW/m^2) at 300 K.
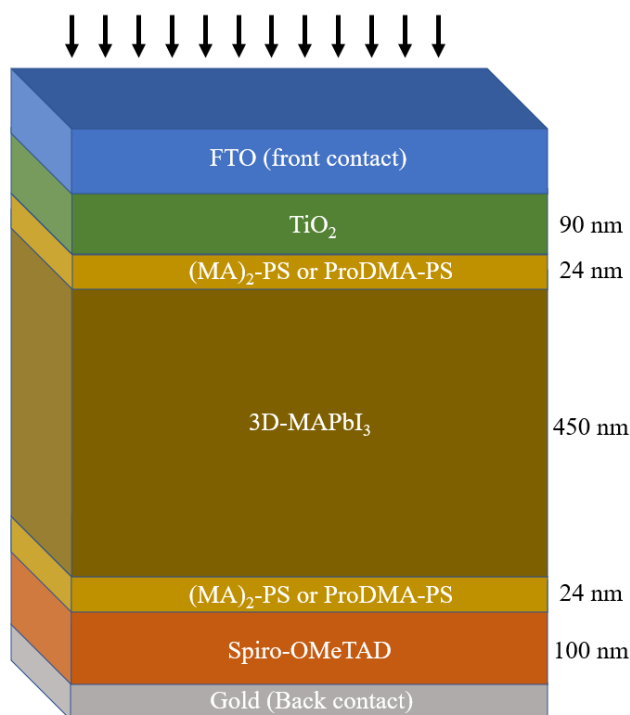

Figure S6 Schematic of the simulated model structure for PSCs.

To get the parameters of the $(MA)_2$-PS and ProDMA-PS, we took them as 2D materials and did the following calculations. The effective conduction band density (N_c) and effective valence band density (N_v) are defined as

$$N_c = \frac{2(2\pi m_n^* k_0 T)^{3/2}}{h^3}$$

$$N_v = \frac{2(2\pi m_p^* k_0 T)^{3/2}}{h^3}$$

where h is Planck's constant, T is the temperature, m_n^* and m_p^* are the effective masses of electrons and holes

$$m_{n/p}^* = \frac{h}{2\pi} \Bigg/ \left[\frac{\partial^2 E_{VBM/CBM}}{\partial k^2}\right]$$

where E is the total energy of the system.

According to the deformation potential theory,[8] the carrier mobility (μ) of 2D materials can be calculated according to the equation[9]

$$\mu = \frac{2eh^3 C}{3(2\pi)^3 k_B T (m^*)^2 (E_1)^2}$$

where e is the electron charge, C is the elastic constant, and E_1 is deformation potential constant. The C and E_1 can be obtained by

$$C = \left[\frac{\partial^2 E}{\partial(\frac{\Delta a}{a_0})^2}\right] \Bigg/ S_0$$

$$E_1 = \frac{\partial E_{edge}}{\partial(\frac{\Delta a}{a_0})}$$

where E_{edge} is the energy of the band edge, Δa is the change of lattice parameter relative to the equilibrium lattice parameter, and S_0 is the area of the unit cell at equilibrium.

Table S1 Simulation parameters of the perovskite solar cells, where d is thickness, E_g is bandgap, χ is electron affinity, ε_r is dielectric constant, N_c is effective conduction band density, N_v is effective valence band density, μ_n is electron mobility, μ_p is hole mobility, N_A is acceptor concentration, N_D is donor concentration, and φ is work function.

Parameter	MAPbI$_3$	TiO$_2$	Spiro-OMeTAD	(MA)$_2$-PS	ProDMA-PS
d (nm)	450	90	100	24	24
E_g (eV)	1.5	3.2	2.9	1.64	1.63
χ (eV)	3.93	4	2.2	3.85	3.86
ε_r	30	100	3	6.27	7.22
N_c (cm^{-3})	2.5×10^{20}	1×10^{21}	2.5×10^{20}	2.97×10^{19}	3.83×10^{19}
N_v (cm^{-3})	2.5×10^{20}	2×10^{20}	2.5×10^{20}	3.23×10^{18}	3.26×10^{18}
μ_n (cm^2/Vs)	50	0.006	0.0021	607	666
μ_p (cm^2/Vs)	50	0.006	0.0026	113	252
N_A (cm^{-3})	-	-	1×10^{18}	-	-
N_D (cm^{-3})	-	5.06×10^{19}	-	-	-
φ (eV)	-	-	5	-	-

Table S2 Parameters of the interface layer

Interface	TiO$_2$ / Light-harvester	Light-harvester / Spiro-OMeTAD
Defect Type	Acceptor	Acceptor
Capture cross section electrons/ holes (cm^2)	1×10^{-17} 1×10^{-18}	1×10^{-18} 1×10^{-19}
Energetic distribution	Single	Single
Reference for defect energy level	Above the VBM	Above the VBM
Energy with respect to Reference (eV)	0.32	0.07
Total density (integrated over all energies) (cm^{-2})	1×10^9	1×10^9

References for the ESI

1   M. J. Frisch, G. W. Trucks, H. B. Schlegel, G. E. Scuseria, M. A. Robb, J. R. Cheeseman, G. Scalmani, V. Barone, G. A. Petersson, H. Nakatsuji, X. Li, M. Caricato, A. V. Marenich, J. Bloino, B. G. Janesko, R. Gomperts, B. Mennucci, H. P. Hratchian, J. V. Ortiz, A. F. Izmaylov, J. L. Sonnenberg, D. Williams-Young, F. Ding, F. Lipparini, F. Egidi, J. Goings, B. Peng, A. Petrone, T. Henderson, D. Ranasinghe, V. G. Zakrzewski, J. Gao, N. Rega, G. Zheng, W. Liang, M. Hada, M. Ehara, K. Toyota, R. Fukuda, J. Hasegawa, M. Ishida, T. Nakajima, Y. Honda, O. Kitao, H. Nakai, T. Vreven, K. Throssell, J. A. Montgomery, Jr., J. E. Peralta, F. Ogliaro, M. J. Bearpark, J. J. Heyd, E. N. Brothers, K. N. Kudin, V. N. Staroverov, T. A. Keith, R. Kobayashi, J. Normand, K. Raghavachari, A. P. Rendell, J. C. Burant, S. S. Iyengar, J. Tomasi, M. Cossi, J. M. Millam, M. Klene, C. Adamo, R. Cammi, J. W. Ochterski, R. L. Martin, K. Morokuma, O. Farkas, J. B. Foresman and D. J. Fox, Gaussian 16, Rev. A.03, Gaussian Inc, Wallingford, CT, 2016.

2   C. T. Lee, W. T. Yang and R. G. Parr, *Phys. Rev. B*, 1988, **37**, 785.

3   A. D. Becke, *Phys. Rev. A*, 1988, **38**, 3098.

4   A. D. Becke, *J. Chem. Phys.*, 1993, **98**, 5648.

5   P. J. Hay and W. R. Wadt, *J. Chem. Phys.*, 1985, **82**, 270.

6   S. Grimme, J. Antony, S. Ehrlich and H. Krieg, *J. Chem. Phys.*, 2010, **132**, 154104.

7   Y. Raoui, H. Ez-Zahraouy, N. Tahiri, O. El Bounagui, S. Ahmad and S. Kazim, *Solar Energy*, 2019, **193**, 948.

8   J. Bardeen and W. Shockley, *Phys. Rev.*, 1950, **80**, 72.

9   N. Wang, M. Li, H. Xiao, H. Gong, Z. Liu, X. Zu and L. Qiao, *Phys. Chem. Chem. Phys.*, 2019, **21**, 15097.